[22]L. F. Mattheiss, J. H. Wood, and A. C. Switendick, in *Methods of Computational Physics* (Academic, New York, 1968), Vol. 8.

[23]This author, however, finds the rule to be somewhat optimistic.

[24]The author has found this observation extremely useful and wishes to express his gratitude for the discussion. The observation is simply that once one has performed the Gaussian elimination to obtain a triangular matrix, one can determine the number of eigenvalues below the energy E by counting the negative signs on the diagonal. This allows one to set up a procedure based on a wide mesh with subsequent iteration to find any number of eigenvalues which might occur with the mesh increment. From Fig. 1, one can see that there are some problems with this simple scheme, but none that cannot be dealt with.

PHYSICAL REVIEW B VOLUME 2, NUMBER 2 15 JULY 1970

High-Frequency dc Haas–van Alphen Oscillations in Aluminum†

J. R. Anderson and S. S. Lane*
Department of Physics and Astronomy, University of Maryland, College Park, Maryland 20742
(Received 16 February 1970)

High-frequency de Haas–van Alphen oscillations attributed to the second-zone Fermi surface have been studied in aluminum. The results have been combined with the lower-frequency values from the third-zone surface measured by Larson and Gordon in order to obtain a three-parameter pseudopotential-interpolation model. The parameters in Rydbergs are $V_{111}=0.018$, $V_{200}=0.062$, and $E_F=0.866_7$. This model has been used to calculate energy bands and a density of states.

I. INTRODUCTION

In recent years many experiments, including studies of the de Haas–van Alphen effect, [1–3] magnetoresistance, [4,5] magnetoacoustic effect, [6] cyclotron resonance, [7,8] and the Kohn effect, [9] have been undertaken in order to investigate the electronic structure of aluminum. These measurements have been consistent with a nearly free-electron Fermi surface. The simplest model of this surface, the single orthogonalized-plane-wave (OPW) or empty-lattice model, consists of three contributions: (i) a large second-zone hole surface (Fig. 1); (ii) a multiply-connected third-zone electron surface; (iii) small fourth-zone pockets of electrons. [10] A more realistic model is obtained by rounding the sharp corners of the empty-lattice model and eliminating the fourth-zone pockets. Detailed experiments, especially de Haas–van Alphen (dHvA) effect studies, have given a rather complete description of the third-zone surface. As shown by Ashcroft[11] a consistent description is obtained if this surface is no longer multiply connected but consists of separated toroid-like surfaces (Fig. 2).

The second-zone surface, however, has been much less completely investigated although ultrasonic attenuation[6] and Kohn effect[9] studies have suggested that the surface approximates the single OPW surface (Fig. 1). The only previous dHvA measurements on this surface have been the pulsed field measurements of Priestley[2] limited to magnetic field orientations along [110] and [111] symmetry directions. Since extremely accurate dHvA measurements are now possible and can be reliably interpreted, we decided to study the high-frequency dHvA oscillations in aluminum (4×10^8–6×10^8 G), related to the second-zone hole surface, and some intermediate frequencies resulting from the third zone. Our measurements combined with the low-frequency measurements of Larson and Gordon[3] have been used to obtain parameters for a four OPW interpolation model, [12] the same type of model as used by Ashcroft. [11]

Even higher-frequency oscillations (1×10^9–1.5×10^9G) have been observed at some orientations and are probably related to magnetic breakdown. Parker and Balcomb[5] observed strong oscillations in the magnetoresistance and suggested that these were due to breakdown between the small pieces of the third-zone surface and the large second-zone hole surface. The highest-frequency dHvA oscillations observed in this investigation have been interpreted in a similar manner.

II. EXPERIMENTAL TECHNIQUES

Measurements of the dHvA effect were made using the low-frequency modification of the field-modulation technique first described by Shoenberg and Stiles. [13] These measurements were normally made at the second harmonic of the 44.3-Hz fundamental frequency. A carefully constructed notch filter[14] (rejection about 80 dB per octave) was

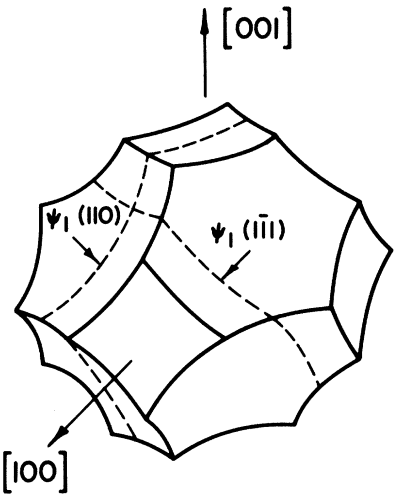

FIG. 1. Second-zone single OPW Fermi surface for aluminum. The dashed lines represent central extremal orbits ψ.

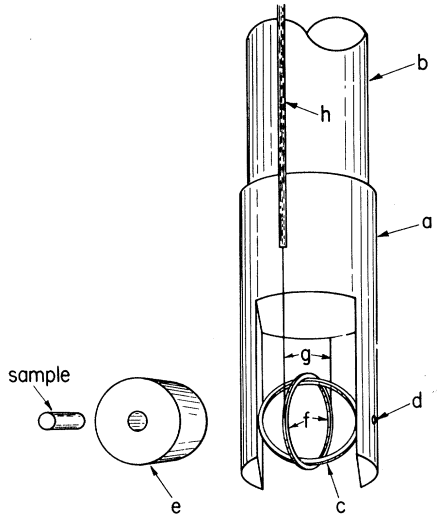

FIG. 3. Rotating sample holder: (a) brass fork; (b) stainless-steel tube; (c) brass ring; (d) Teflon bushing; (e) pickup coil; (f) outer brass ring; (g) 0.007-in. soft stainless-steel wire; (h) stainless-steel rod.

used to remove the fundamental from the pickup signal, which had been stepped up by a transformer. The resulting output was detected with a lock-in amplifier and displayed on a strip chart recorder.

A typical pickup coil consisted of two concentric sections wound in opposition with about 6000 turns on the inner part and 2000 turns on the outer. The main purpose for this compensation was to minimize noise voltages caused by mechanical vibrations of the system. The modulation field was produced by a solenoid which slipped over the fork (a) (Fig. 3) described below. A modulation amplitude of typically 5-G peak was used to study the high-frequency oscillations.

The dc magnetic field was produced by a Westinghouse 55-kG superconducting solenoid (coil constant about 3.3 kG/A) with homogeneity better than 3 parts in 10^5 over a $\frac{1}{2}$-in.-diam sphere. The field was measured by reading the voltage across a small resistor (~0.02 Ω) in series with the magnet; calibrations were made using the Al^{27} NMR resonance in metallic aluminum [$\gamma = 11.1119$ MHz/(10 kG)]. As a result of a rather comprehensive study of hysteresis effects made over an extended period of time, we believe our field measurements in this study are accurate to slightly better than 0.1%.

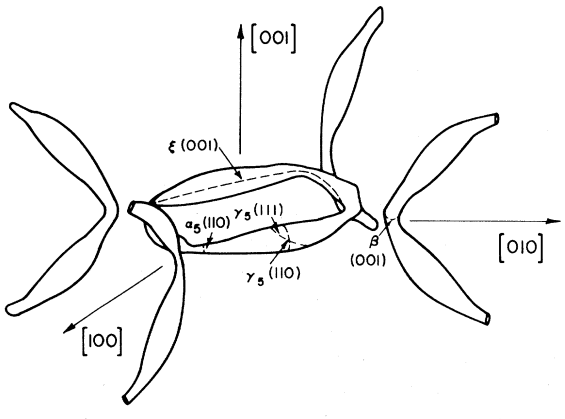

FIG. 2. Model of third-zone toroidal Fermi surface, after Ashcroft (Ref. 11). The dashed lines indicate extremal orbits.

The rotating sample holder is shown in Fig. 3. The balanced pickup coil (e) was slipped inside the ring (c) which rotated inside the fork (a) on teflon bushings (d). An outer ring (f) slipped over the first ring (c) and was driven by the stainless steel wire (g). One end of the wire was attached to the rod (h), whose position was controlled by a micrometer head outside the Dewar. The other end was attached to a spring at the top of the helium cryostat.

The pickup coil could be rotated with respect to the ring (c) so as to orient the desired plane of rotation to better than $1\frac{1}{2}^\circ$ and a desired symmetry axis to better than $\frac{1}{2}^\circ$. The rotation system was calibrated at room temperature by measuring the angular deflection of a beam of light reflected from a mirror attached to the ring (f), and tabulating

this angle against the micrometer setting. By this means it was found that the sample rotated 1° for each 5.71 thousandths of an inch of micrometer travel, and that this rate was constant over the full range of travel. The micrometer head was driven by a variable speed motor when it was desired to rotate the sample in a fixed field. The field was held constant to better than 0.5 G/h by operating the magnet in the persistent mode.

We have estimated the over-all accuracy of our frequency measurements at symmetry directions [110] and [111] to be about 0.3%. This includes errors in magnetic field measurements, about 0.1%, and statistical limitations on cycle counting, about 0.1%. There are also complications arising from the mixing of dHvA frequencies, but we believe that errors resulting from this effect are negligible at symmetry directions. (For nonsymmetry directions errors are considerably greater, not only due to the complicated pattern of oscillations but also due to the smaller amplitude.) The position of closest approach to a symmetry axis was determined accurately by looking for symmetry in the dHvA frequency pattern during sample rotations at constant magnetic field. Thus the orientation error at symmetry directions is estimated to be less than $1\frac{1}{2}°$ and the resulting contribution to the error should be less than 0.1%.

III. SAMPLE PREPARATION

The starting materials used in these investigations were both 99.9999% purity aluminum obtained from Cominco[15] and a large single-crystal boule of resistivity ratio about 2×10^4 which was given to us by Dr. R. Powell of the NBS Cryogenics Laboratory in Boulder, Colo. Our best single crystals were grown by means of the Czochralski method[16] of pulling from the melt and these gave dHvA signals perhaps 100 times stronger than those from crystals spark cut from the NBS boule. (We have not yet tried pulling with the NBS boule as the melt.) The crystals formed were about 0.050 in. in diameter and several inches long. With care they could be made quite uniform in diameter. They were cut into 0.4-in. lengths with a spark cutter, polished in hot phosphoric acid, and and mounted directly in the pickup coil. One end of the sample was secured with Apiezon N-type vacuum grease. In spite of the care taken in mounting, the samples were usually appreciably degraded by thermal cycling.

IV. RESULTS

The experimental results will be presented in terms of the extremal second- and third-zone orbits suggested by the empty-lattice model. From the second zone (Fig. 1), in addition to the central orbit ψ_1, there are noncentral but still extremal orbits, labeled ψ_2, at most orientations of the magnetic field. From the third zone there are orbits α, β, and γ, corresponding to arm cross sections, and an orbit ξ around the inside of the toroid formed by four arms (Fig. 2).[17]

dHvA oscillations were obtained both by sweeping the field at fixed sample orientations and by rotating the sample at constant field. Frequencies attributed to the third-zone Fermi surface were observed at all orientations, but were easily distinguished from those from the second zone which were a factor of about 150 higher. We have not studied the third band in any detail but have relied upon the measurements of Larson and Gordon[3] to obtain our Fermi-surface model. However, in order to compare our results with theirs, we have made an absolute determination of the frequency corresponding to the γ_5 orbit for $\vec{H}\|[110]$. Our value is $F_\gamma = 2.85 \pm 0.015 \times 10^6$ G, which is in good agreement with the Larson and Gordon value of 2.86×10^6 G.

The beat pattern in the high-frequency oscillations in aluminum is fairly simple. When the signals were of large amplitude, for example, near [110] and [111], two frequencies, differing by about 3%, were present, giving rise to beats of about 33 cycles in the dominant frequency. In addition, at many orientations long beats of 150 or more cycles were observed due to the influence of the third-zone Fermi surface. An example of this beating is shown in Fig. 4.

Frequencies measured in the (110) plane by the field-sweep method are shown in Fig. 5. Those measured in the (100) plane by the angular-sweep method using a constant magnetic field (~40 kG) are shown in Fig. 6. The angular-sweep method gives only frequency differences; at the starting point $\vec{H}\|[110]$, the frequency was measured accurately with a field sweep of about 2000 cycles. High-frequency dHvA oscillations were not observed at all field orientations, primarily because of sample perfection problems and a magnetic field limited to about 55 kG. Although signals were strong near the symmetry directions [110] and [111], it was only with the best samples, which had not been thermally cycled between 300 and 4 °K more than once, that oscillations could be observed at other orientations. Thus with the three samples studied in these investigations (two with axes along [100] and a poorer quality sample with axis along [111]), we were able to investigate only the range of orientations shown in Figs. 5 and 6.

The solid lines in both figures correspond to the single OPW calculation and it can be noted that the angular variation predicted by this model agrees quite well with the data even though the actual

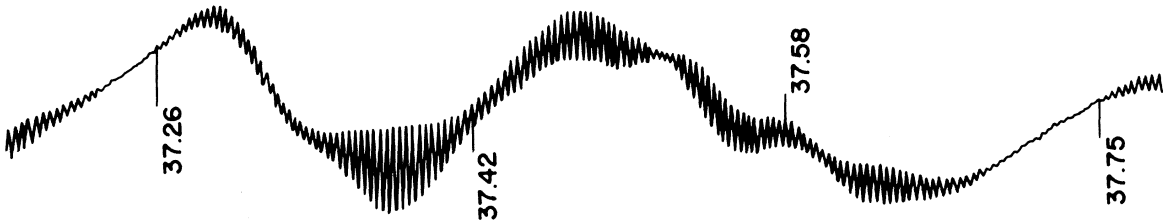

FIG. 4. High-frequency dHvA oscillations for $\vec{H} \parallel [110]$. The field marker spikes represent the field values in kG. Long beats of about 150 cycles are present as well as shorter beats of 20 to 40 cycles.

magnitudes differ by from 5 to 10%. Near the [100] axis, oscillations (ξ) of about 0.9×10^8 G were observed over an angular range of about $2\frac{1}{2}°$. These oscillations were of such large amplitude as to mask the higher-frequency oscillations at [100], which have very small amplitude. Although it should be possible to adjust the modulation amplitude to get rid of the ξ oscillations near [100] in order to study the higher frequencies expected from the hole surface, we have not yet been able to do this successfully. We have, however, observed oscillations from the hole surface to within about 1° of [100].

Some frequencies measured at symmetry directions in this work are shown in Table I. (The value from the [100] holes has been obtained by extrapolation.) Also shown are the three frequency values measured by Priestley[2] using pulsed fields. Priestley's values are in agreement with ours within the combined experimental errors. The lower frequencies shown in Table I were measured by Larson and Gordon[3] and were used in fitting to the Fermi surface as discussed in Sec. V.

Additional frequencies up to 1.5×10^9 G (Fig. 7) were observed at some orientations in aluminum, corresponding to areas larger than any cross section of the Brillouin zone (see Fig. 8). In most cases these could not be interpreted as harmonics or combinations of known dHvA frequencies, and so we have attributed them to magnetically induced transitions between different portions of the second-zone surface, perhaps using parts of the third

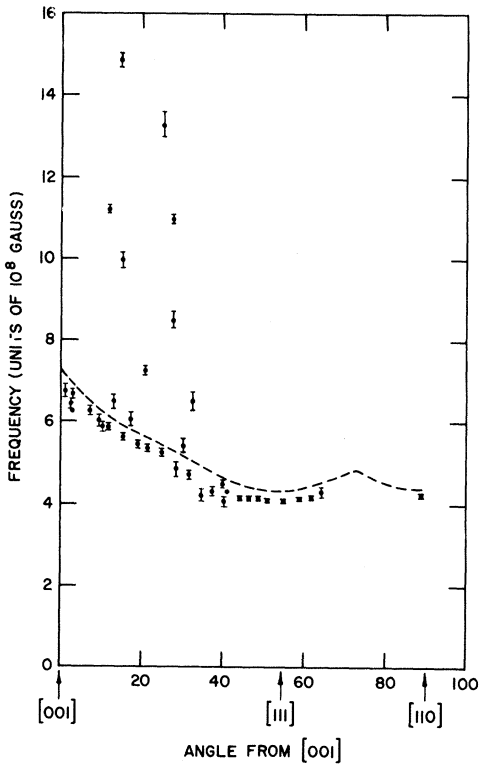

FIG. 5. Experimental dHvA frequencies versus magnetic field direction for rotation in an (011) plane. The dashed line shows the single OPW calculation. The higher-frequency values for H roughly 20° from [001] have been attributed in part to magnetic breakdown orbits.

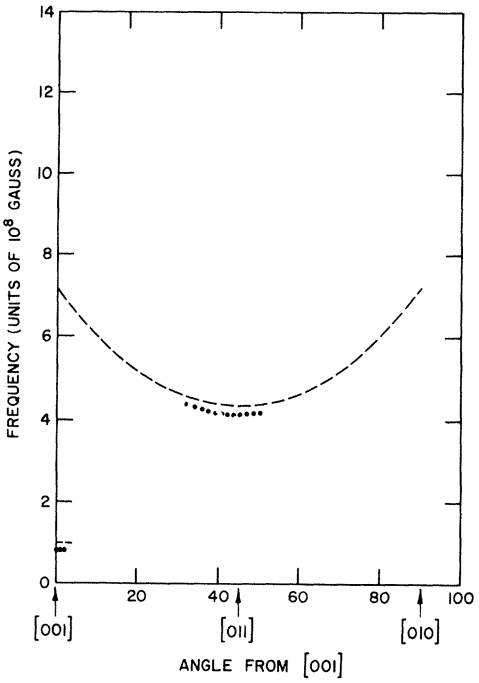

FIG. 6. Experimental dHvA frequencies versus field direction for rotation in the (100) plane. Since away from [110] the amplitude decreased rapidly, oscillations were studied over only a limited angular range. The dashed line represents the single OPW calculation.

zone surface as a bridge. These are a subject of further investigation at present.

V. THEORETICAL DESCRIPTION OF FERMI SURFACE AND COMPARISON WITH EXPERIMENT

Harrison[10] showed that the OPW method, with parameters determined by fitting to energies at symmetry points as calculated by Heine, predicted a third-zone Fermi surface for aluminum which was roughly consistent with experimental results from the dHvA effect, cyclotron-resonance effect, and anomalous-skin effect. Then Ashcroft,[11] using the low-frequency dHvA data of Gunnerson to determine aluminum pseudopotential parameters, obtained a third-zone Fermi surface which was quantitatively slightly different from that proposed by Harrison. In particular, he found that the symmetry point W[18] was not occupied by third-zone electrons and thus the third zone was made up of disconnected toroidal rings. Neither of these calculations took into account any experimental data due to the second-zone surface, although both predicted a second-zone surface very close to the free-electron result. It was hoped that inclusion of some dHvA areas from the second zone might yield pseudopotentials which would provide a better fit to the entire Fermi surface.

We have combined our second-zone dHvA measurements with the lower-frequency third-zone measurements of Larson and Gordon[3] in order to determine a model of the Fermi surface. For this purpose a three-parameter pseudopotential-interpolation model has been used which is identical to that used by Ashcroft[11] for aluminum and similar to that used by Anderson and Gold[19] for lead. Two of the parameters used were the first two Fourier coefficients of the pseudopotential V_{111} and V_{200}. (V_{000} has no effect upon the shape of the Fermi surface.) In addition, the Fermi energy E_F was adjusted so that the requirement of 3 electrons/atom would be maintained. In this calculation the two Fourier coefficients were assumed to be independent of the wave vector $\vec{k}$ (local model). Four OPW's are degenerate at the point W in the empty-lattice model, the maximum degeneracy that arises in the energy range considered here; this is the main reason for the explicit inclusion of only four OPW's in our calculation.

TABLE I. dHvA frequencies and cross-sectional areas at symmetry directions.

Orbit	Axis	Freq (10^6 G)	Area in units of $(2\pi/a)^2$ Measured	Empty lattice	Three-parameter model
ψ_1	[110]	436.6 ±0.6 (431 ±1) [a]	1.709 ±0.002	1.728	1.698
ψ_1	[111]	411 ±1 (417 ±3)[a]	1.609 ±0.008	1.898	1.623
ψ_1	[100]	680 ±20[b]	2.66 ±0.08	2.84	2.60
ξ	[100]	88.8 ±0.2	0.3472 ±0.000 3	0.3501	0.347 4
γ_5	[110]	2.85 ±0.015	0.0112 ±0.000 1	0.0212	0.011 14
γ_5	[111]	3.44 ±0.04[c]	0.0135 ±0.000 2	0.0254	0.013 55
β	[100]	0.46_6 ±0.02[c]	0.00182 ±0.000 08	•••	0.001 79

[a] Priestley (Ref. 2).

[b] This frequency was obtained by extrapolation and was omitted from the least-squares fitting calculation.

[c] Larson and Gordon (Ref. 3). The error estimates are those used in our least-squares calculation; no errors were given explicitly in Ref. 3.

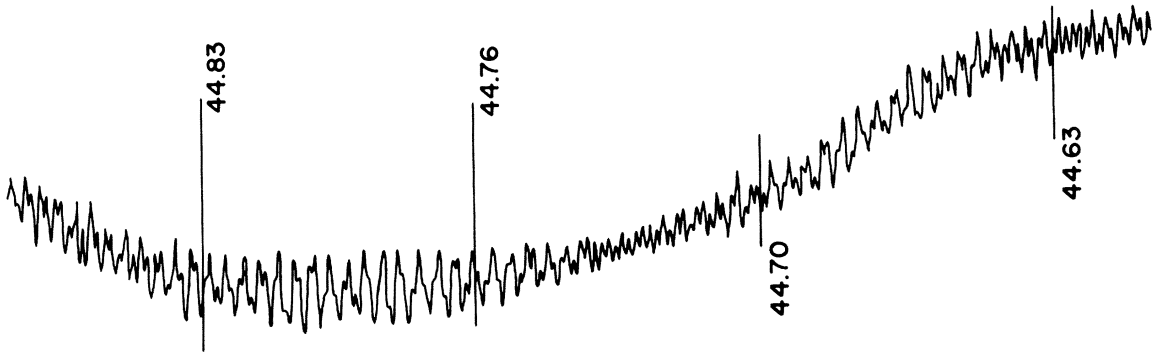

FIG. 7. High-frequency dHvA oscillations $27\frac{1}{2}^\circ$ from [100] in a (011) plane. The marker spikes represent field values in kG. At least five frequencies are present.

In the region near $W(\frac{1}{2}, 0, 1)$[20] the four OPW's are labeled by $\vec{k}$ vectors $\vec{k}_i = \vec{k} - \vec{K}_i$, $i = 0, 1, 2, 3$, where $\vec{K}_i$ are reciprocal-lattice vectors, $\vec{K}_0 = 0$, $\vec{K}_1 = [002]$, $\vec{K}_2 = [111]$, and $\vec{K}_3 = [1\bar{1}1]$; $\vec{k}$ is the specific point in the Brillouin zone. Thus the truncated Hamiltonian matrix $\mathcal{H}$, which is of order four, becomes

$$\mathcal{H} = \begin{pmatrix} T_0 & V_{200} & V_{111} & V_{111} \\ V_{200} & T_1 & V_{111} & V_{111} \\ V_{111} & V_{111} & T_2 & V_{200} \\ V_{111} & V_{111} & V_{200} & T_3 \end{pmatrix} . \qquad (1)$$

Here T_i are the kinetic-energy terms $\hbar^2 k_i^2/2m^*$ and we have chosen m^* to be the free-electron mass; the shape of the Fermi surface does not depend upon the value chosen for this quantity.

Constant energy surfaces were traced out by choosing an energy E and finding values of $\vec{k}$ that solved the secular equation resulting from Eq. (1). In order to extend the calculation throughout the entire Brillouin zone, the zone was divided into 24 equivalent regions and the set of OPW's was automatically changed as $\vec{k}$ crossed from one region into another. This procedure has been described by Anderson and Rhyne.[21]

Since we wished to compare with the dHvA measurements, we calculated the areas enclosed by orbits on the Fermi surface. The Fermi energy depends, of course, upon the values of V_{111} and V_{200}, and must be determined for each set of parameters by integrating to find the volume enclosed within the constant energy surface. In practice this did not prove to be too difficult, as the initial guess of the free-electron energy was quite close to the final value.

The dHvA frequencies corresponding to six orbits (see Table I) were used in a least-squares calculation in order to determine the values of the parameters V_{111}, V_{200}, and E_F. The six dHvA frequencies resulted from orbits in high-symmetry planes and were chosen because they were the most accurately measured and because their combination was considered to be a representative sample of the entire Fermi surface. These frequencies were converted to cross-sectional areas using the relation $\mathcal{A} = 3.915 \times 10^{-9} F$, where $\mathcal{A}$ is given in units of $(2\pi/a)^2$ and F is the dHvA frequency in Gauss. [$\mathcal{A}$ (Å^{-2}) $= 0.0549 \times 10^8 F$(Gauss).]

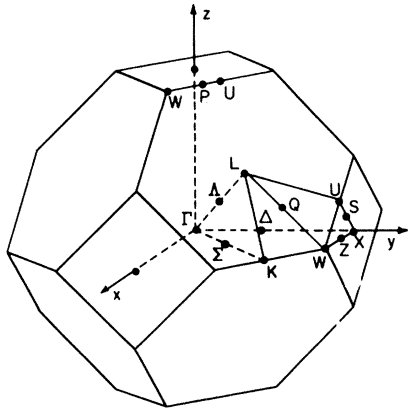

FIG. 8. Fundamental Brillouin zone for a fcc metal. The symmetry points are labeled according to the convention of Bouckaert *et al.* (Ref. 18).

The parameters, in Rydbergs, determined by the least-squares fit are

$$V_{111} = 0.018, \quad V_{200} = 0.062, \qquad E_F = 0.866_7 (E_F^0 = 0.8695). \tag{2}$$

Here E_F^0 is the single OPW Fermi energy which is only slightly larger than our value. For comparison, Ashcroft's parameters, in Rydbergs, are $V_{111} = 0.0179$, $V_{200} = 0.0562$, and $E_F = 0.85605$. However, Ashcroft probably used the room-temperature lattice constant value ($a = 4.04$ Å) since his free-electron Fermi energy was 0.86057 Ry.

The restriction to 3 electrons/atom has been included, although the accuracy of the volume calculation for our model was only about 0.1%. (This accuracy was limited by the amount of computer time used in the calculation.) The ratio V_{200}/E_F (= 0.0715) is in reasonable agreement with the results of Mina *et al.* ($V_{200}/E_F \approx 0.066 \pm 0.005$)[22] estimated from the deviation of the measured cyclotron mass from the single OPW result. Our calculated areas are also shown in Table I. Since the rms deviation of the theory from the experiment for the six orbits of Table I is about 1%, the agreement may be regarded as good. Only the β[100] area differs from experiment by more than 1%, and since this area is quite sensitive to the parameters, small changes in V_{111}, V_{200}, or E_F could greatly improve the agreement for this orbit, while having little effect on the other parts of the Fermi surface.

Our model could probably be improved by including other contributions such as spin-orbit coupling or additional OPW's. However, it is expected that a spin-orbit term would give only a small contribution to the Fermi surface of such a light metal as aluminum. Adding another OPW explicitly would also seem to be inappropriate. The V_K pseudopotential components found here were developed by following a procedure which removes a degeneracy in first order. However, when we determine the best parameters by experiment we actually find, instead of V_K, the quantity[23]

$$V_K + \sum_{K' \neq K} \frac{V_{K'-K} V_{K'}}{E_K - E_{K'}} \quad . \tag{3}$$

Therefore, all the other V_K's are actually included to second order. At the point $U(\frac{1}{4}, \frac{1}{4}, 1)$, for example, both $V_{\bar{1}11}$ and $V_{1\bar{1}1}$ contribute equally to the energy, but we have used only $V_{1\bar{1}1}$ explicitly. Thus $V_{\bar{1}11}$ is included only in the sense of expression (3), introducing an error which might limit the inherent accuracy of the model's fit. We have calculated the [110] arm central cross section including directly this fifth OPW ($\vec{K}_4[\bar{1}11]$) and the main result is an increase in this area by about 10%. Although this correction is appreciable, the [110] arm cross section is probably the worst case and we have elected to neglect this contribution in our complete fitting calculation. A desirable characteristic of the OPW model is its simplicity and its near approximation to the free-electron model, and this simplicity begins to be lost when too many adjustable parameters or OPW's are included, or when it takes excessive computer time to trace out the Fermi surface. Thus we have retained what we believe to be the simplest model giving reasonable agreement with experiment.

As an additional check on our model, we have calculated the minimum (110) arm cross section to be $1.06 \times 10^{-3}\ (2\pi/a)^2$. This corresponds to a frequency of 0.265×10^6 G, in good agreement with the value of 0.26×10^6 G measured for the α oscillations by Larson and Gordon.[3]

Calculated and measured frequencies in the (110) and (100) planes are shown for the second-zone hole surface in Figs. 9 and 10, and it can be seen that the experimental points are virtually indistinguishable from the calculated curve when the measurement uncertainty is included. The central orbit for the second-zone surface is extremal at all orientations. In addition, the presence of beats of from 30 to 40 cycles near [110] and [111] suggests the existence of noncentral extremal hole orbits. It has not been possible to determine whether the second frequency, indicated by the presence of these beats, is greater than or less than the dominant frequency due to the central sections and therefore these experimental results have not been included in Figs. 9 and 10. However, the noncentral orbit areas have been calculated for our model and are shown in Figs. 9 and 10. The angular range of existence of these orbits is less than that predicted by the empty-lattice model and the beats observed near [110] and [111] tend to disappear near orientations where our model predicts the absence of these noncentral extremal sections. Thus, we believe the beats we have observed are evidence of noncentral sections of the second-zone hole surface.

The case of the orbit ξ in the third zone is more clearcut (see Fig. 2). Angular rotation data suggest that this orbit disappears 2.5° from [100] in the (001) plane, and this agrees very well with the computed range of 3°. In a (110) plane the oscillations disappear about $1\frac{1}{2}$° from [001], while the calculated angle is about 2°.

Further evidence that the rings of arms do not connect at W has been obtained from a search for additional dHvA frequencies near [111]. If an orbit on the inside of a ring of third-zone arms in a

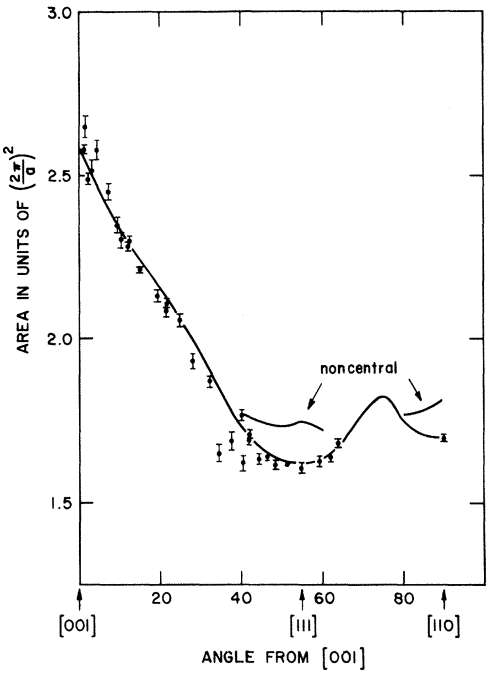

FIG. 9. Cross-sectional areas of the Fermi surface determined from measured dHvA frequencies for rotation in a $(1\bar{1}0)$ plane. Higher-frequency oscillations shown in Fig. 5 have not been included. The solid lines represent the values calculated from the three-parameter model for both central and noncentral extremal sections of the second-zone hole surface.

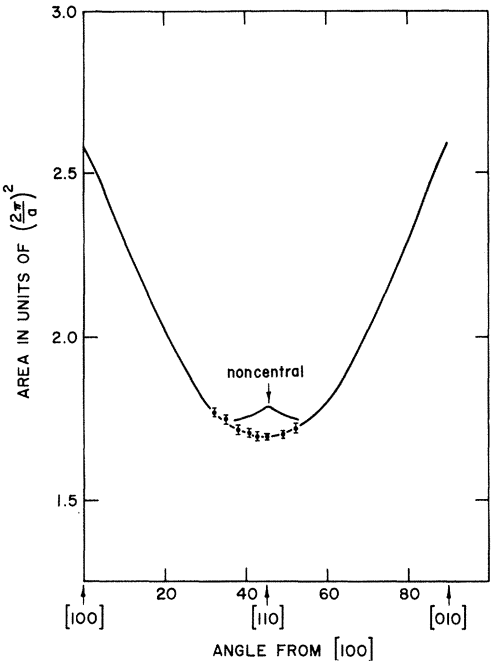

FIG. 10. Cross-sectional areas of the Fermi surface determined from measured dHvA frequencies for rotation in an (001) plane. The solid lines represent the values calculated from the three-parameter model for both central and noncentral extremal sections of the second-zone hole surface.

(111) plane existed, it should lead to oscillations with amplitude comparable to those due to the orbit ξ and these should be easily visible as beats of about three cycles in the high-frequency [111] oscillations. Such beats were not observed either in this work or that by Priestley.

dHvA *Amplitudes*. In a metal such as aluminum, where the magnetoresistance tends to saturate so that eddy currents are important, the dHvA amplitude may not follow a simple Bessel function relationship.[24] In order to check this point, we have made a few measurements of dHvA amplitudes resulting from second-zone orbits ($F = 4.36 \times 10^8$ G) as a function of the modulation amplitude h_m as shown in Fig. 11 for a dc magnetic field of about 45 kG parallel to [110]. The solid line is calculated from the simple Bessel function expansion for the second harmonic $CJ_2(2\pi F\kappa h_m/H^2)$. Here F is the dHvA frequency and H is the applied dc magnetic field. C is a constant obtained by fitting at the first amplitude maximum. The value of κ is 0.23, determined by fitting the argument of J_2 at the first zero. In the absence of eddy currents κ would be one. We note that all the zeros are fitted quite closely by this expression, but the experimental amplitude falls off much more rapidly with modulation than the Bessel function. Thus

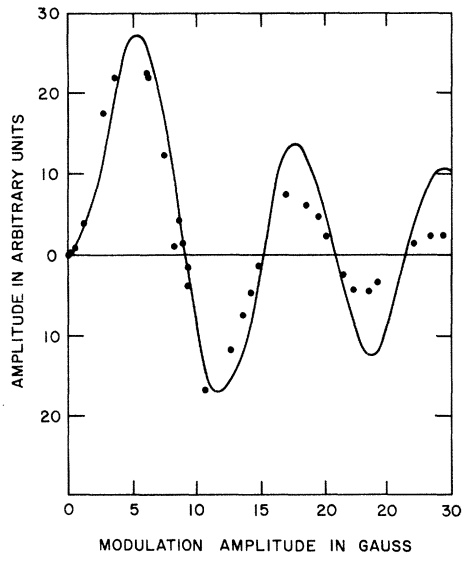

FIG. 11. dHvA amplitude versus modulation field for H in [110] direction ($F = 4.366 \times 10^8$ G). H is approximately 46 kG. The solid line is calculated from the Bessel function $J_2(2\pi F\kappa h_m/H^2)$ where $\kappa = 0.23$. The Bessel function is multiplied by a constant in order to fit the first amplitude maximum.

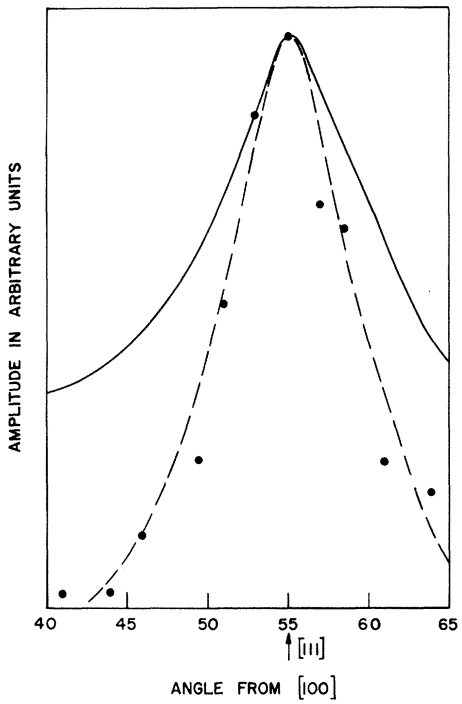

FIG. 12. dHvA amplitude of high-frequency oscillations ($F \sim 4.1 \times 10^8$ G) versus angle. The solid line is calculated for a constant Dingle temperature at 0.75 °K. The dashed line is calculated for an assumed microstructure with random variation of the order of 0.01°.

the Bessel function expression must be modified to include the effects of eddy currents in order to agree with our experimental amplitudes. Some calculations have been made including this effect for the parallel plane geometry.[25]

Figure 12 shows the dependence of dHvA amplitude on angle near the [111] direction. The points are not intended to represent absolute amplitudes but to illustrate the general behavior of the amplitude. The terms affecting the angular dependence of the amplitude are the dHvA frequency, the effective mass, and the curvature factor $d^2\alpha/dk_z^2$. We have used the effective-mass values of Spong and Kip,[8] Fermi-surface curvatures calculated on our model, and an assumed constant Dingle temperature of 0.75 °K to calculate the solid lines of Fig. 12. The solid line has been fitted to the data at the maximum amplitude at [111]. One can see that the experimental amplitudes fall off much more rapidly than the calculated values. One possible explanation is that the samples may have a microcrystalline structure. If the sample consists of microcrystals whose axes have a small angular spread, the dHvA signal will be the result of averaging over an appropriate range of phases. This range of phases will be the smallest when the frequency has a stationary value with respect to angle, as in the [111] direction, and therefore the dHvA amplitude will be larger at [111] than in its neighborhood. To estimate this effect, a knowledge of the distribution of microcrystals is required, and we have not made such a determination for our crystals. However, if we assume a Gaussian distribution of microcrystalline axes about [111], following the approach of Priestly,[2] our amplitude measurements would imply that the substructure has a random variation of the order of 0.01°. The dashed line in Fig. 8 shows the results of making this correction and the agreement is now quite satisfactory.

Effective masses measured at symmetry orientations in this work and by Spong and Kip,[8] using cyclotron resonance, are shown in Table II. Also shown are masses predicted from our model. Another second-zone measurement is due to the dHvA measurements of Priestley, who found a hole mass of $1.3m_0$ for H in the [111] direction. There is good agreement between our measurements and those of Spong and Kip.[8] The scaling factor giving the ratio between the measured masses and band masses is between 1.5 and 1.7. This is about the same as the third-zone scaling factors determined by Larson and Gordon[3] except that they give a factor of only 1.3 for the γ oscillations. The discrepancy between the observed masses and those calculated on the OPW model is observed in many experiments and has been attributed primar-

TABLE II. Cyclotron masses.

		m^*/m_0 Measured		m^*/m_0 Calculated		m_{obs}/m_{calc}	
Orbit	Axis	dHvA	Cyclotron resonance (Ref. 7)	Empty lattice	Three-parameter model	dHvA	Cyclotron resonance
ξ	[100]	0.84 ± 0.07	0.8	0.4	0.5	1.68	1.6
ψ_1	[100]	1.30 ± 0.1	1.27	0.82	0.82	1.59	1.55
ψ_1	[111]	1.36 ± 0.1	1.40	0.93	0.89	1.52	1.57

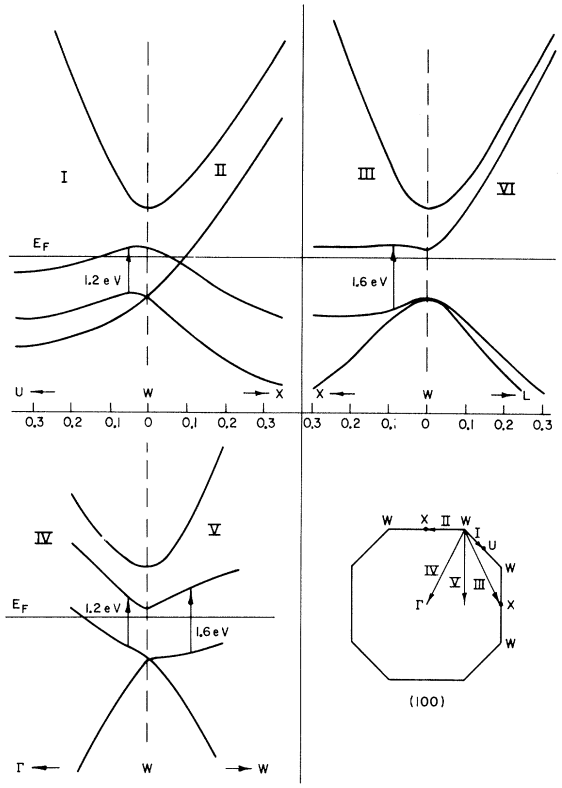

FIG. 13. Energy bands near W calculated from the three-parameter model. The arrows show energy differences of 1.2 or 1.6 eV and indicate our interpretation of regions contributing to the optical peaks.

ily to electron-phonon interactions.[26] This effect may be taken into account in an approximate way by replacing the kinetic terms $\hbar^2(\vec{k}+\vec{K})^2/2m$ in Eq. (1) by $\alpha\hbar^2(\vec{k}+\vec{K})^2/2m$, where α is estimated to be about $\frac{2}{3}$. This correction changes the kinetic energy and therefore the mass of the electrons, but not the shape of the Fermi surface itself.

With the parameters chosen to fit dHvA results [Eq. (2)], we have calculated the band structure near the Fermi surface. The results are very similar to those shown by Ashcroft[11] and consequently we present only the energy values at symmetry points in Table III. From this table we note that there are no third-band electrons at the symmetry point W, showing that the third band is not multiply connected. Therefore, we would expect no open orbits in aluminum, and consequently saturation of the magnetoresistance at all orientations of magnetic field. This result would appear to contradict the measurements of Parker and Balcomb[5] who find that the resistance depends linearly upon magnetic field at high fields. However, they explain their results by assuming that magnetic breakdown occurs at high fields and this explanation is consistent with our observation of very high-frequency oscillations, some of which we attribute to magnetic breakdown.

TABLE III. Energy levels at symmetry points (in eV).

Γ	X	U	L	W
37.2	19.48	19.87	25.90	12.96
28.7	17.77	11.39	25.36	11.98
27.1	10.12	10.29	7.16	10.79
0	8.47	9.63	6.71	10.79

Optical experiments have shown absorption peaks at about 1.2 and 1.6 eV in aluminum.[27] Both peaks can probably be explained by interband transitions near W (see Fig. 13). The 1.2-eV peak may result from transitions in the immediate vicinity of W, while the 1.6-eV transitions take place slightly farther from W, for example, for initial state $\vec{k}$ vectors lying in the [111] Brillouin-zone faces.

As part of the calculation of optimum model potential parameters, it has been necessary to calculate volumes enclosed by constant energy surfaces. From these results the density of states $\mathfrak{N}(E)$ has been determined (Fig. 14). Only the third-zone electrons and second-zone holes contribute over the small energy range shown. It

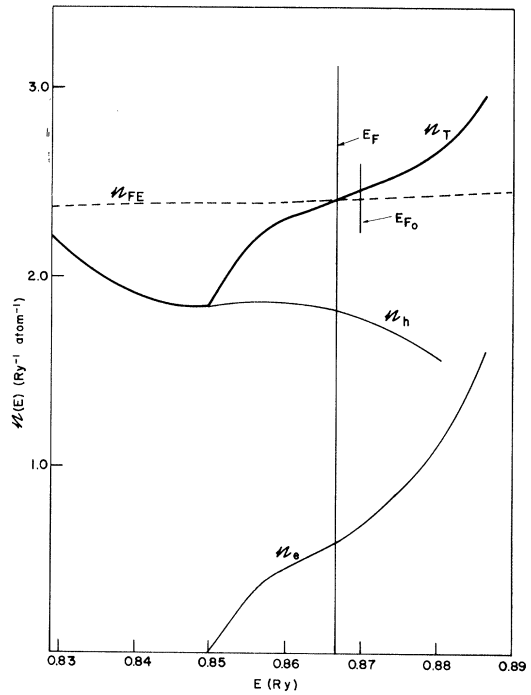

FIG. 14. Density of states $\mathfrak{N}_T$ and Fermi energy E_F calculated from the three-parameter model. $\mathfrak{N}_h$ and $\mathfrak{N}_e$ represent the second-band hole and third-band electron contributions to the density of states, respectively. The diagram shows only the energy region over which the first band is full and the fourth band is empty. The dashed line shows the free-electron density of states.

can be seen that the model predicts almost the same value for the density of states at the Fermi surface $\mathfrak{N}(E_F)$ as that resulting from the single OPW model; the slope $\mathfrak{N}'(E_F)$ is greater, however. The density of states determined from low-temperature electronic specific-heat measurements[28] is about 1.6 times the calculated $\mathfrak{N}(E_F)$ agreeing well with the mass enhancement results, as expected.

VI. SUMMARY

From the third-zone low-frequency dHvA experiments of Larson and Gordon[3] and our second-zone high-frequency dHvA measurements, we have determined two Fourier coefficients of a local pseudopotential. With this potential we have calculated a Fermi surface in good agreement with experiment. In addition, the band structure and density of states near the Fermi energy have been obtained.

ACKNOWLEDGMENTS

We especially acknowledge the help given to this project by Dr. D. C. Hines, who calibrated the superconducting magnet. We are indebted to him and Dr. D. R. Stone for many helpful conversations. The support of the University of Maryland Computer Science Center is gratefully acknowledged.

Note added in proof. Bos and Lynch [L. W. Bos and D. W. Lynch (unpublished)] have also measured optical absorption in aluminum and have not observed the structure at 1.2 eV but have found a peak at about 0.5 eV. (Dresselhaus *et al.*[27] did not make measurements down to 0.5 eV.) Both Dresselhaus [G. Dresselhaus (private communication)] and Brust [D. Brust, Phys. Letters 31A, 289 (1970)] have calculated the dielectric function for aluminum using the Ashcroft parameters. They find absorption peaks at energies of about twice the values of the pseudopotential parameters, that is, at about 0.5 and 1.6 eV, but they find no structure near 1.2 eV. Since our parameters are nearly the same as those of Ashcroft, a calculation of the dielectric function using our parameters also would be expected to show no structure at 1.2 eV. It is not clear at the present time whether a discrepancy exists between experiment and calculation, but both need further study.

---

†Work supported by the Advanced Research Projects Agency. Parts of this paper are based upon a thesis submitted by Dr. Lane in partial fulfillment of the requirements for a Ph.D. in Physics, University of Maryland, College Park, Md.

*Present address: Environmental Research Corp., 813 North Royal Street, Alexandria, Va.

[1]E. Gunnerson, Phil. Trans. Roy. Soc. London A251, 85 (1958).

[2]M. G. Priestley, Phil. Mag. 7, 1205 (1962).

[3]C. O. Larson and W. L. Gordon, Phys. Rev. 156, 703 (1967).

[4]E. S. Borovik and V. G. Volotskaya, Zh. Eksperim. i Teor. Fiz. 48, 1554 (1965) [Soviet Phys. JETP 21, 1041 (1965)].

[5]R. A. Parker and R. J. Balcomb, Phys. Letters 27A, 197 (1968).

[6]G. N. Kamm and H. V. Bohm, Phys. Rev. 131, 111 (1963).

[7]T. W. Moore and F. Spong, Phys. Rev. 125, 846 (1962).

[8]F. Spong and A. F. Kip, Phys. Rev. 137, A431 (1965).

[9]R. Stedman and G. Nilsson, Phys. Rev. Letters 15, 634 (1965).

[10]W. A. Harrison, Phys. Rev. 118, 1182 (1960).

[11]N. W. Ashcroft, Phil. Mag. 8, 2055 (1963).

[12]cf. W. A. Harrison, *Pseudopotentials in the Theory of Metals* (Benjamin, New York, 1966), pp. 100–116.

[13]D. Shoenberg and P. J. Stiles, Proc. Roy. Soc. (London) A281, 62 (1964).

[14]G. E. Valley and H. Wollman, *Vacuum Tube Amplifiers* (McGraw-Hill, New York, 1948), p. 348.

[15]Cominco American, Inc., 818 West Riverside Avenue, Spokane, Wash.

[16]J. Czochralski, Z. Physik. Chem. 92, 219 (1917).

[17]For the low-frequency oscillations attributed to the third zone we have used the notation of Larson and Gordon (see Ref. 3).

[18]Symmetry points in the Brillouin zone such as W and U refer to the standard nomenclature as given by L. Bouckaert, R. Smoluchouski, and E. Wigner, Phys. Rev. 50, 58 (1936).

[19]J. R. Anderson and A. V. Gold, Phys. Rev. 139, 1459 (1965).

[20]We give all dimensions in k space in units of $(2\pi/a)$ where a is the lattice constant at low temperatures $\{a = 4.02$ Å [R. W. Armstrong (private communication)]$\}$.

[21]J. R. Anderson and M. K. Rhyne, U.S. Atomic Energy Commission Research and Development Report No. IS-1106, 1965 (unpublished).

[22]R. T. Mina, V. S. Edel'man, and M. S. Khaikin, Zh. Eksperim. i Teor. Fiz. 51, 1363 (1966) [Soviet Phys. JETP 24, 920 (1967)].

[23]M. H. L. Pryce, Proc. Phys. Soc. (London) A63, 25 (1950).

[24]R. W. Stark and L. R. Widnmiller, Cryogenics 8, 272 (1968).

[25]R. A. Johnson, M. S. thesis, Iowa State University, 1967 (unpublished).

[26]N. W. Ashcroft and J. W. Wilkins, Phys. Letters 14, 285 (1965).

[27]G. Dresselhaus, M. S. Dresselhaus, and D. Beaglehole, Proceedings of the Electronic Density of States Conference, National Bureau of Standards, Gaithersburg,

Md. (to be published).
[28]J. G. Daunt, in *Progress in Low Temperature Physics*, edited by C. J. Gorter (North-Holland, Amsterdam, 1955).

PHYSICAL REVIEW B VOLUME 2, NUMBER 2 15 JULY 1970

Study of the Interaction of Light with Rough Metal Surfaces. I. Experiment*

D. Beaglehole and O. Hunderi

Department of Physics and Astronomy, University of Maryland, College Park, Maryland 20742
(Received 23 September 1969)

This paper describes measurements of the reflectivity, scattering, and transmission of light by metals with rough surfaces. For surfaces whose roughness is very short ranged, the ratio of rough-surface reflectivity to smooth-surface reflectivity varies exponentially as λ^{-2} both above the plasmon frequency and in regions where $\epsilon_2 \gg |\epsilon_1|$. In the latter regions for these rough surfaces, the scattered intensity follows a λ^{-4} wavelength variation. For surfaces which are more wavy, the reflectivity and scattered light vary less rapidly with wavelength. Well below the plasmon frequency, additional fields not present on smooth surfaces, but coming from induced extra currents and dipoles on rough surfaces, add coherently to the specular beam, with a resonant wavelength variation. Near the plasmon frequency there is extra absorption. We have studied the angular variation of the scattered light, and have observed additional incoherent light associated with these extra dipoles and currents. We compare the experimental results with the scalar scattering theory and make some general comments about the properties of surface dipoles and currents.

I. INTRODUCTION

Light reflected from a smooth homogeneous surface is found only in the specular beam, and its intensity, given by Fresnel's equations, depends upon the polarization of the incident light, the angle of incidence, and the dielectric properties of the bulk medium. When light is reflected from rough surfaces, two new phenomena occur. Firstly, the condition of specularity is relaxed and scattered light is found away from the specular beam, with a reduction in the specular intensity. Fresnel's equations are no longer valid. Secondly, additional currents may be excited, and dipoles induced across pits and bumps on the surface. These can give rise to additional fields which mix with the specular and scattered intensities.

Early theories of the reflection of light from rough surfaces have neglected the effects of additional currents and dipoles. The best-known theory is the "scalar scattering" theory.[1] This considers just the phase modulation of the incident and outgoing light by the height variations along the surface. The specular and scattered light are found by summing the radiation from Huygens wavelets on the surface. The radiation distribution thus depends upon the phase of the wavelets – determined by the phase of the incident field when it reaches a point of the surface – and upon their correlation over the surface. If the height variation is assumed to be normally distributed about its mean with an rms deviation σ, the scalar scattering theory predicts the ratio of the specular reflectivity of a rough surface to that of a smooth surface to vary as $R_r/R_s = e^{-(4\pi\sigma/\lambda)^2}$, and the theory similarly makes predictions about the angular distribution of the scattered light. The scalar scattering theory is energy conserving – all the light lost from the specular beam should appear in the scattered distribution. However, the approximations of the development in Ref. 1 are such that this is only so if the typical distance for variation along the surface a is of the order or greater than λ.

The scalar scattering theory is a simple approach to the interaction of light with rough metal surfaces. It neglects the vector nature of the radiation field and it neglects the distortion of the incident and outgoing fields near the local surface.

A new approach is that of Twersky[2] and Berreman.[3] These authors have considered models representing rough surfaces, models in which it is possible to solve exactly for the electromagnetic fields. The models have consisted of randomly distributed hemispherical bosses, pits, and closely associated shapes on otherwise smooth surfaces. These calculations have been made in